IOSR Journal Of Applied Physics (IOSR-JAP)
e-ISSN: 2278-4861.Volume 17, Issue 5 Ser. I (Sept – Oct 2025), PP 48-56
www.Iosrjournals.Org

Reviewed Study Of A NIM PET/CT Phantom To Evaluate PET Image Quality In Detection Of Micro-Lesions Comparing With NEMA IEC Body Phantom And Performance Parameters Of CT

Elmubarak Mohamedahmed, Rasool Kattubadi, Majeed Rowaily
Consultant Medical Physicist Medical Physics Unit, Medical Imaging Department, King Abdualaziz Medical City Riyadh,
A Senior Medical Physicist, Medical Physics Unit, Medical Imaging Department, King Abdualaziz Medical City Riyadh.
A Head Of Medical Imaging Department, King Abdualaziz Medical City Riyadh,

Abstract
Background: *Reviewed the previous study with commonly used NEMA IEC Body phantom, we observed that it has a number of defects, hindering its application for detecting micro-lesions and measuring the performance parameters of computed tomography (CT). This study aimed to propose a PET/CT phantom designed by National Institute of Metrology (NIM), China, which is capable of simultaneously testing the performance of PET and CT systems, and to evaluate the quality of imaging.*
Methods: *The phantom was developed in the current study, the NIM PET/CT phantom, is composed of a PET imaging module and a CT imaging module, and these modules are connected together through bolts, which can simul- tenuously measure the imaging performance of PET and CT systems and similar to NEMA IEC Body phantom. Hot spheres were filled with 4:1 sphere-to- background activity concentration using 18F-fluorodeoxyglucose (18F-FDG), and cold spheres were filled with non- radioactive water. The results of imaging obtained from the NIM PET/CT phantom and the NEMA IEC Body phantom were compared to assess their diagnostic efficacy. In order to evaluate the generalization ability of the NIM PET/CT phantom, three different PET/CT systems were used to scan on the same scanning protocol. To evaluate the effects of image reconstruction algorithms on image quality assessment, VPFX (Vue point FX), VPHD (Vue point HD), ordered subset expectation maximization (OSEM), OSEM-point-spread function (PSF), OSEM-TOF, and OSEM-PSF-TOF algorithms were employed using Discovery MI Gen2, 3 ring scanner (GE).*
Results: *The imaging quality of the NIM PET/CT phantom and the NEMA IEC Body phantom was relatively consistent. The NIM PET/CT phantom could detect 7 mm spheres without influencing the imaging quality. It was found that PSF reconstruction exhibited to reduce the speed of convergence, the contrast and background variability of spheres (13–28 mm) were significantly improved after two iterations. In addition to improve the image contrast and background variability, TOF could markedly improve the overall image quality and instrument detection limit. TOF-PSF could noticeably reduce noise level, enhance imaging details, and improve quality of imaging.*
Conclusions: *The results showed that in comparison with the NEMA IEC Body phantom, the NIM PET/CT phantom outperformed in evaluating the PET image quality of micro-lesions and the performance parameters of CT.*
Keywords: *NEMA IEC Body phantom, NIM PET/CT phantom, CT performance parameters, Image quality, Hot spheres, Cold spheres, Micro-lesions.*

Date of Submission: 14-09-2025 Date of Acceptance: 24-09-2025

I. Background (Introduction)

Positron emission tomography (PET) has proven invaluable in the diagnosis, staging, and treatment response evaluation of a broad range of tumors. The technologies adopted and refined in PET systems mainly address basic imaging parameters, such as resolution, sensitivity, and aperture, influencing the overall quality of PET images. X-ray computed tomography (CT) is based on differential absorption of X-ray by different tissues to enable distinction between different anatomical structures, and the CT uses sophisticated mathematical techniques to construct a two-dimensional (2D), three-dimensional (3D) images. With the development of medical imaging techniques, fused image with a large amount of information for increasing the clinical applicability of medical images. In initial staging, PET/CT exhibited a higher sensi tivity in detecting distant metastases compared to conventional imaging, leading to disease upstaging and the consequent switch from a local approach to a systemic chemotherapy [2].

In medical imaging, physical phantoms refer to real objects designed to simulate the human body for specific clinical conditions. Physical phantoms are used to calibrate imaging systems, evaluate their performance, and ensure the correct operation of imaging systems before scanning human subjects. They also constitute an inexpensive way of testing new imaging applications and serve as a well-defined reference for quantitative measurements. Because of the differences in contrast from one region to another, images typically show a clear

delineation of internal structure (anatomy), morphology, and physiological functions. In 1994, the National Electrical Manufacturers Association (NEMA) published the NEMA NU2-1994 standard for performance assessment of PET. Thereafter, the NEMA NU2 standard and the IEC61675-1 standard issued by the International Electrotechnical Commission (IEC) have been repeatedly

revised. According to the NEMA NU 2–2012 standard, image quality parameters of PET scanners could be obtained by measuring a specific IEC-61675–1 emission phantom i.e. NMEA IEC Body phantom, This image quality phantom mimics the shape of an upper human body and is built of acrylic glass. The PET component of the PET/CT system can be evaluated using the method described in the NEMA standard, and the CT component is mainly associated with the low contrast resolution. [1].

Although PET-NEMA/IEC body phantom is widely used, it still has a number of shortcomings. Firstly, the minimum inner diameter of spheres used to measure image quality parameters in phantom is 10 mm, thus, the phantom cannot meet the requirements of detecting micro lesions. Secondly, the mentioned phan- tom can only be applied to PET measurement. The third limitation is the requirement of specific temperature and humidity conditions for storage, to ensure the standardized use of phantom for repeated measurements and in multicenter trials. Hence, the present study aimed to pro- pose a PET/CT phantom designed by National Institute of Metrology (NIM), China, which we have designed, tested their basic model with 7mm smallest sphere and is capable of simultaneously testing the performance of PET and CT systems, and to evaluate image quality.

Institute of Metrology (NIM), China, which is capable of simultaneously testing the performance of PET and CT systems, and to evaluate quality of imaging [1].

II. Methods

The NEMA IEC body phantom

The NEMA IEC Body phantom is an anthropomorphic phantom recommended by both NEMA and IEC, and it is extensively utilized in PET imaging. This phantom mimic the shape of an upper human body and is built of acrylic glass material. It comprises 6 hollow glass spheres (inner diameters of 37, 28, 22, 17, 13, and10 mm), which can be inserted into the large phantom compartment. Additionally, a cylindrical insert containing styrofoam with an average density of 0.3 ± 0.1 g/ml, and is positioned in the center of the phantom. The NEMA IEC Body phantom simulates hot and cold lesions and reflects the clinical image quality of a PET/CT system. It two largest spheres (diameters of 37 and 28 mm) as the cold lesions and the other spheres (diameters of 22, 17, 13, and 10 mm) as the hot lesions. Besides, a cylindrical lung inserts, filled partly with a low atomic number material with an average density of 0.30 ± 0.10 g/ cc was used (Fig. 1).

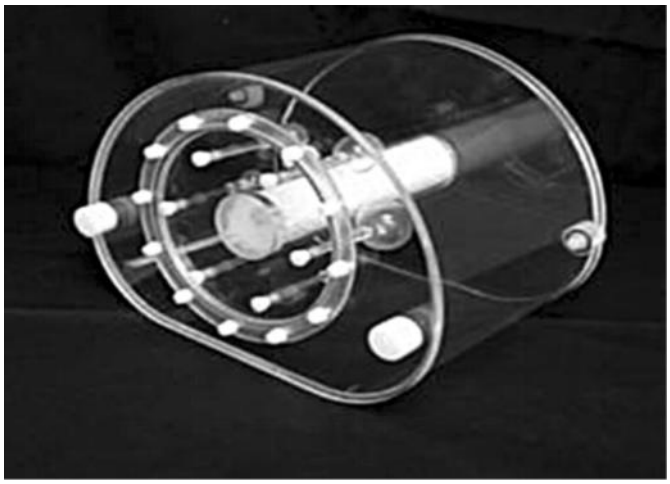

Fig. 1 The NEMA IEC Body phantom

The NIM PET/CT phantom

The phantom developed in the present study is composed of a PET imaging module and a CT imaging module, and these modules are connected together through bolts. This phantom can simultaneously assess the imaging performance of PET and CT systems (Fig. 2).

The structure of a PET imaging module in the NIM PET/CT phantom was found similar to that of the NEMA IEC Body phantom, in which filling was performed by ^{18}F fluorodeoxyglucose (F-FDG) solution. It comprises 6 hollow glass spheres (inner diameters of 37, 28, 22, 17, 13, and 10 mm), a cylindrical lung insert. In addition to the 6 hollow spheres specified in the NEMA NU2 standard, 2 hollow spheres with diameters of 4 and 7 mm were added.

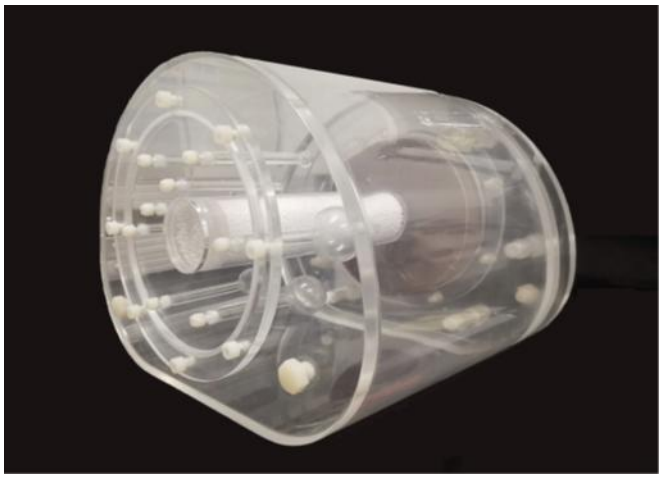

Fig. 2 The NIM PET/CT phantom

Among them, spheres with diameters of 28 and 37 mm were filled with purified water for cold lesions, and the remaining (inner diameters of 22, 17, 13, 10, 7, and 4 mm), were filled with 18F-FDG solution for hot lesions. The distribution of spheres in the proposed phantom is shown in (Fig. 3).

The CT imaging module was developed with a diameter of 150 mm and a thickness of 20 mm. The background was filled with purified water, and was made of a nonmetallic CT-free artifact material, which was equivalent to water. Besides, three low-contrast CT inserts with the same diameter were inserted, with a triangle distribution, whose low-contrast resolution was 0.5%, 1.0% and 1.5%, respectively.

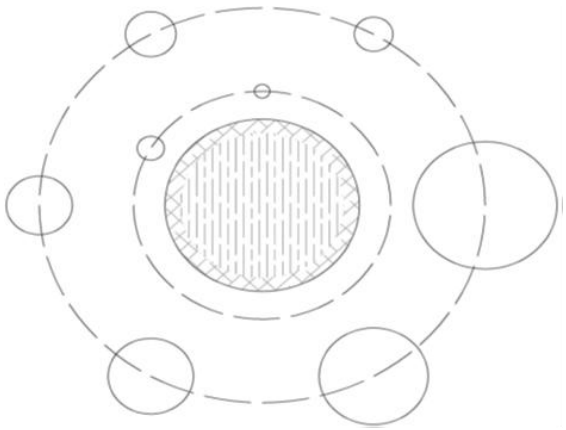

Fig. 3 The distribution of spheres in the NIM PET/CT phantom.

Image quality control

Region of interest (ROI)

ROIs were placed on PET and CT images. ROIs of PET images included cold spherical ROIs, hot spherical ROIs, spherical ROIs, and lung insert ROI; ROIs of CT images involved internal ROIs and background ROIs. Twelve ROIs (37 mm) are drawn on the background region. Background ROIs for spheres with diameters of 10, 13, 17, 22, and 28 mm are drawn concentric to the ROIs (37 mm) as indicated in the top background ROI.

All spherical ROIs were drawn on slices centered on the spheres and background ROIs with the same size and concentric distribution was on the background at the same level. Besides, ROIs were drawn on slices as close as possible to ± 1 and ± 2 cm on each side of the central slice. A total of 60 background ROIs, including 12 ROIs on each of five slices, were accordingly drawn (Fig. 4). Lung ROIs were drawn in form of a circle with a diameter of 30 ± 2 mm on the center of the simulated lung tube. ROIs of CT images included internal ROIs of each insert and the same background ROIs (n = 3) around each insert (Fig. 5).

PET image analysis

The contrast recovery coefficient (CRC) is the percentage of measured net concentration normalized by the measured background concentration to true net concentration normalized by true background concentration. CRC provides information of how accurately the system reproduces the true activity concentration in a specific volume. CRC for hot sphere is was calculated following cold, background ratios.

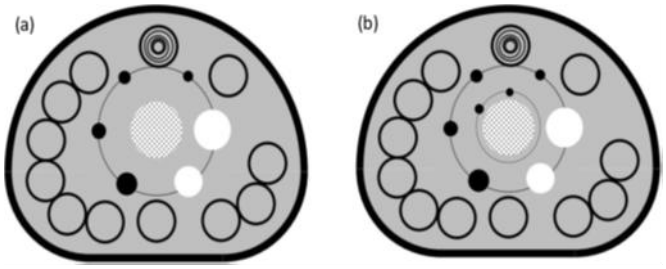

Fig. 4 The layout of background ROIs for PET image quality analysis in (a) NEMA IEC Body phantom and (b) NIM PET/CT phantom.

Percentage of background variability

The percentage of background variability calculated following standard deviation (SD) of the activity concentration in the background ROI.

Measurement of the residual error using CT-based attenuation and scatter-corrected PET images.

To measure the residual error using CT-based attenuation and scatter-corrected PET images, the relative error was calculated for each slice by calculating the ratio of the average counts in the lung insert ROI to the average counts in the background ROIs. Percentage of misplaced counts in the lung insert, following the NEMA NU 2-2012 guidelines.

CT images with low-contrast resolution

CT images with a low-contrast resolution were presented by calculating differences in CT values, in which differences with 15, 10 and 5 HU between CT values indicated that1.5%, 1.0% and 0.5% of CT images had a low-contrast resolution, resolution respectively.

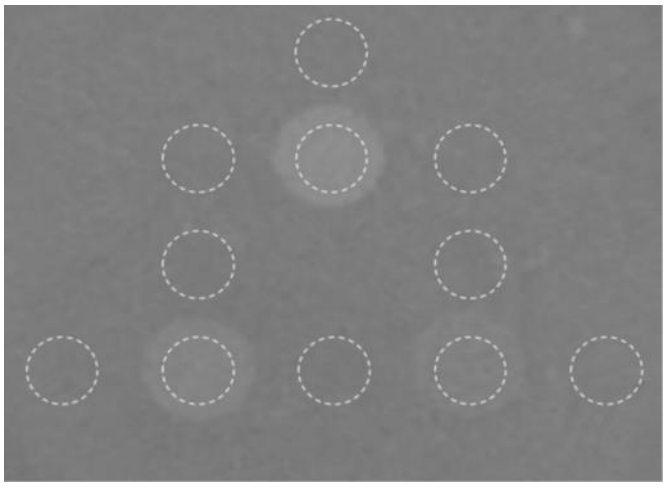

Fig. 5 The layout of background ROIs for CT image quality analysis.

Data acquisition

Hot spheres were filled with 4:1 sphere-to-background activity concentration using 18F-FDG, and cold spheres were filled with non-radioactive water for cold lesions. Place the phantom on the patient table after effective assembly, and scanning was started immediately after positioning. Whole-body spiral CT scan was performed with a matrix of 512 × 512, pixel size of 1.417 × 1.417 mm, a slice thickness of 2.78 mm, and a tube voltage of 140.00 kV (Helical, full 70cm). Besides, PET acquisition time was about 8 min (Table 2).

Image reconstruction

Generally, the performance parameters of PET and the visibility of lesions in phantoms are strongly dependent on parameters of the reconstruction algorithms. In PET, positron range and inter-crystal scattering can affect measurement resolution, and each can be modeled within system matrix. However, the calculation of such factors within the system matrix impacts the speed of computation and the convergence of the algorithm.

During investigation of novel scenarios in PET, the accuracy of the system matrix can be chosen to reflect the application of the system and the speed required during image reconstruction. All PET images were reconstructed with the matrix size of 256 × 256 and the image dimensions 384 x 384 x 53, VPFX reconstruction (Table 1).

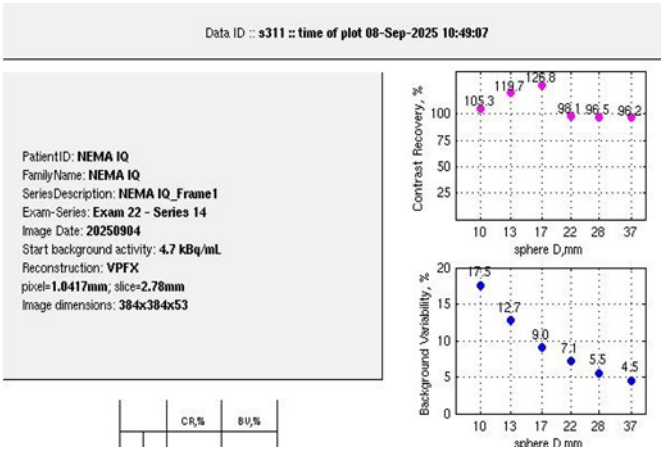

(Figure 6) Image Reconstruction

The PET data were reconstructed primarily using the VPFX, VPHD, ordered subset expectation maximization (OSEM) algorithm, and the number of iterations was 2. The main motivation for time of-flight (TOF)-PET has always been the potential image quality improvement or reduction in image acquisition time of TOF-PET. TOF-PET data can be easily compared with PET data for the same study as the TOF data can be ignored during reconstruction. The point-spread function (PSF)reconstruction produces images with the improved isotropic spatial resolution, the reduced ratio of spill-in/spill-out, and the increased activity concentration in micro lesions that can be more easily detected and characterized. In order to evaluate the effects of TOF-PET on image quality assessment, VPFX, VPHD, OSEM, OSEM-PSF, OSEM-TOF, and OSEM-PSF-TOF algorithms were employed. The PET reconstruction conditions are showed in (Table 3).

Table 2 Comparing the measurement parameters of the NIM PET/CT phantom and NEMA IEC Body phantom

	NIM PET/CT phantom	NEMA IEC Body Phantom
CB (kBq/mL)	6.2	6.2
CH (kBq/mL)	25.6	25.6
A (kBq)	60,820	61,510
T (min)	8	8

CH, the mean activity concentration in the hot spheres; *CB*, the mean activity, concentration in the background; A, the total activity; T, PET imaging time

Table 3 PET reconstruction conditions (**2 iterations**)

Phantom	Algorithm	Matrix	Pixel size (mm)	Thickness (mm)
NIM PET/CT phantom	VPFX, VPHD, OSEM OSEM-PSF OSEM-TOF OSEM-PSF-TOF	256 x 256	1.417	2.78
NEMA IEC body phantom	VPFX, VPHD, OSEM-PSF-TOF	256 x 256	1.417	2.78

III. Results

PET-dependent parameters for image quality assessment was undertaken for both cold and hot lesions with different sizes to provide an indicator for the detection of lesions. A number of factors, such as emission scan duration, 18F-FDG activity concentration, target-to-background activity concentration ratio, and body mass index of the scanned object can affect CRC and background variability, identified as PET image quality descriptors. The attenuation correction strategies can be divided into (a) methods based on image segmentation, (b) machine learning methods, and (c) data-driven approaches, utilizing PET data alone or in synergy with existing CT data. The lower the residual error is, the higher accuracy of attenuation correction of the PET/CT system is.

The NIM PET/CT phantom and NEMA IEC Body phantom were used to assess the quality of PET images with the same PET/CT system and the same scanning protocol. Figure 7 shows a similar quality of PET images by both NIM PET/CT phantom and NEMA IEC Body phantom, indicating that the measurement results of the two phantoms would be comparable to some extent. Besides, the NIM PET/CT phantom was designed with 2 smaller spheres (4 and 7 mm), and a 7 mm sphere could be observed in the 10 o'clock direction of the phantom image, which could evaluate the imaging quality of PET/CT in micro lesions.

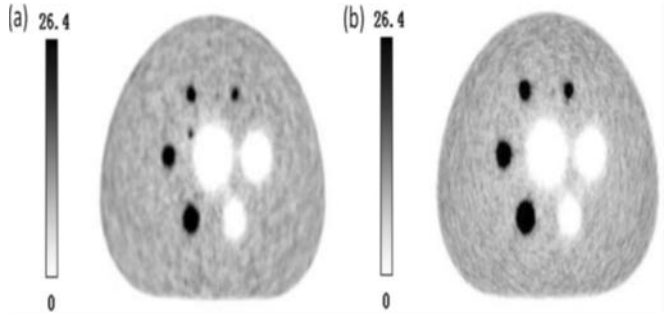

Fig. 7 PET images of (a) NIM PET/CT phantom and (b) NEMA IEC Body phantom

As presented in Table 3 (a), 3 (b) showing measured ratios in between contrast vs background in the NIM PET/CT phantom, NEMA IEC Body phantom and NIM PET/CT Phantom images could measure the quality of PET images and accurately estimate the residual error using the CT-based attenuation and scatter-corrected PET images according to the current standards, and the added spheres slightly influenced the contrast, background variability, and residual error (deviation is 0.14%).

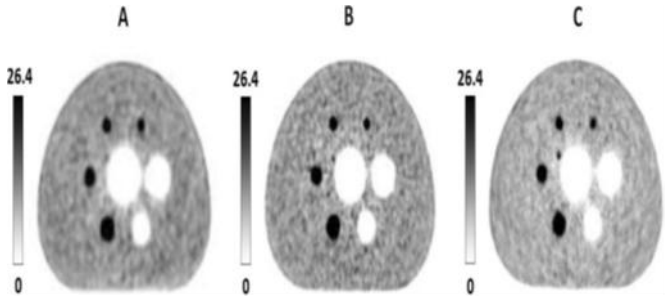

Fig. 8 *PET reconstruction images of the NIM PET/CT phantom on different systems*

Table 3(a) *Image Quality PET-dependent parameters for NIM PET/CT phantom (Deviation is* ***0.14****%)*

Description	Sphere (mm)	Measured Ratio
Image Quality		**4:1**
% Contrast for each hot sphere	7mm	19.21
	10mm	44.52
	13mm	62.80
	17mm	70.52
	22mm	73.11
% Contrast for each cold sphere	28mm	85.71
	37mm	96.2
% Background variability	7mm	6.11
	10mm	5.66
	13mm	4.53
	17mm	3.95
	22mm	3.27
	28mm	2.89
	37mm	2.5

Accuracy of attenuation and scatter corrections		
% Relative error for each lung slice	50mm	14.6
Accuracy of radioactivity quantitation		
Radioactivity concentration in KBq/mL	Background	4.5
	Hot sphere	N/A

Table 3(b) *Image Quality PET-dependent parameters for NEMA IEC Body phantom*

Description	**Sphere (mm)**	**Measured Ratio**
Image Quality		**4:1**
% Contrast for each hot sphere	10mm	44.52
	13mm	66.73
	17mm	72.04
	22mm	72.93
% Contrast for each cold sphere	28mm	85.71
	37mm	95.62
	10mm	5.13
	13mm	4.57
	17mm	3.91
	22mm	3.11
	28mm	2.56
	37mm	2.14
Accuracy of attenuation and scatter corrections		
% Relative error for each lung slice	50mm	13.9
Accuracy of radioactivity quantitation		
Radioactivity concentration in KBq/mL	Background	4.5
	Hot sphere	N/A

CT-dependent parameters for image quality assessment

The low-contrast module of the NIM PET/CT phantom contained 3 inserts with the low-contrast resolution of 1.5%, 1.0% and 0.5%, respectively, which could meet the measurement requirements of different PET/CT systems.

ROIs with an equal size were drawn inside and around each insert (Fig. 5), CT values within each ROI were measured, and then, differences in CT values, SD, and CNR were calculated (Table 4). The results were in a good agreement with the truth values. The CT values and the SD values in the background ROIs around the same insert were similar, thus the background uniformity was satisfactory. Moreover, due to the good water-equivalent characteristic of the background materials, the background is almost integrated with purified water for injection (Fig.8). In order to quantify the water-equivalent characteristic of the background, 8 ROIs with an equal size were selected to verify the imaging characteristic at the boundary between purified water and the background was calculated (Table 4). According to the measurement results, the SD was relatively small (maximum SD is 3.61 HU as the bold number showed), indicating that the CT value smoothly varied at the boundary and degree of water-equivalence in the phantom was satisfactory.

To further understand the performance of an integrated CT system, CT values were respectively measured in the background and the boundary between the background and purified water (Fig. 9), and the CT values in the main ROI and in the four ROIs were recorded. The CT values at the boundary were found similar and relatively stable, and the uniformity of CT under background, boundary and purified water mode respectively.

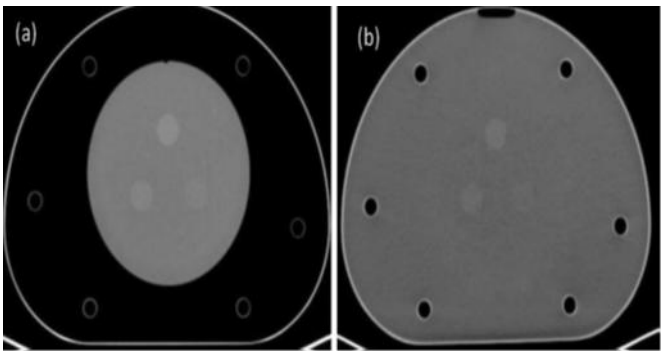

Fig. 8 The verification of water-equivalent characteristic in the background of low-contrast CT module for injection of purified water. (a) Before, (b)after

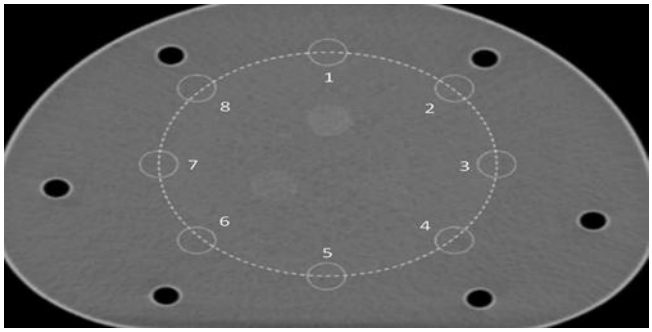

Fig. 9 Noise measurement at the boundary between purified water and background. The circles 1–8 represent ROIs 1–8

Comparison of image reconstruction algorithms

In order to compare the image quality of NIM PET/CT phantom under different reconstruction algorithms, four different algorithms (primarily VPFX, VPHD, OSEM, OSEM-PSF, OSEM-TOF, and OSEM-PSF-TOF) were applied to reconstruct PET images with a PET/CT system. It was revealed that PSF-TOF significantly improved the resolution and the contrast of spheres. However, when only PSF was used, the edge of spheres remained vague. Besides, TOF effectively improved the edge of spheres, reduced noise level, and detected more details for imaging. In order to assess the level of improvement of image quality achieved by a reconstruction algorithm, the image contrast and background variability were calculated, and plotted as a linear graph. It was found that PSF reduced the noise level and enhanced the image contrast. However, since PSF reconstruction exhibited to reduce the speed of convergence, the contrast and background variability of spheres (13–22 mm only) were significantly improved after two iterations. In terms of 37 mm, 28 mm and 10 mm spheres, PSF influences little on image contrast. In addition to improve the image contrast and background variability, TOF showed to greatly elevate the overall image quality and instrument detection limit.

***Table 4 Results** of noise measurement at the boundary between purified water and background **(Number in bold is the maximum SD**)*

ROIs	ROI-1	ROI-2	ROI-3	ROI-4	ROI-5	ROI-6	ROI-7	ROI-8
SD (HU)	3.41	3.42	3.51	**3.61**	3.36	3.45	3.26	3.33

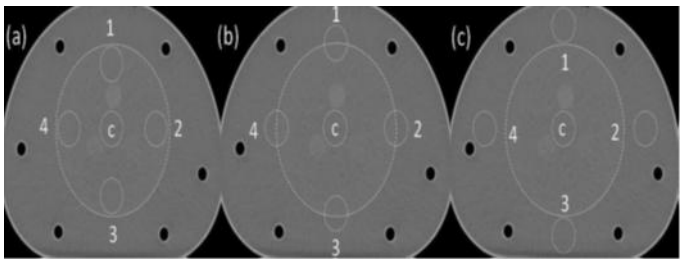

Fig. 10 CT value acquisition for image uniformity for (a) background of CT module, (b) boundary between background and purified water, and (c)pure water area. The circles 1–4 represent ROIs 1–4, and the circle "c" represents "ROI-c"

IV. Discussion

The principle of PET imaging is the detection of gamma rays, originating from the annihilation of positrons with electrons within the examined object. Positron emitters with short half-life are labelled to specific biological molecules and injected into patients. Depending on the carrier molecule, the radioisotope is distributed across different body tissues, providing physiological information from the ROI. Therefore, a critical requirement for designing a PET imaging phantom is the feasibility to simulate radiotracer activity similar to that expected in clinical PET studies.

The present study proposed the PET/CT phantom for evaluating the PET image quality of micro-lesions, which is composed of a PET imaging module and a CT imaging module, and it can simultaneously detect the quality of PET/CT images. The minimum detectability is one of the most important tasks in a PET system, which is directly associated with the early diagnosis and staging of lesions. The minimum inner diameter of spheres used to measure parameters related to image quality in the NEMA IEC Body phantom is 10 mm according to the international guidelines. The physical size of a lesion is practically difficult to derive from PET images due to pill-out and partial volume effects. Thus, in clinical studies, the quantification is generally based on the maximum voxel value or the mean value inside a three-dimensional (3D) contour.

V. Conclusions

In summary, this reviewed study significantly improves performance in detection of microlesions using NIM PET/CT phantom and in comparison, with NEMA IEC Body phantom, and also influence of Computed Tomography parameters. However, suggested further research needs to be carried out for the proposed phantom. We have gone thru previous articles and did this comparison study to evaluate above results.

Abbreviations

NEMA: National Electrical Manufacturers Association; PET: positron emission tomography; IEC: International Electrotechnical Commission; CT: computed tomography; NIM: National Institute of Metrology; 18F-FDG: 18F-fluorodeoxyglucose; TOF: time-of-flight; OSEM: ordered subset expectation maximization; PSF: point spread function; 2D: two-dimensional; ROI: region of interest; CRC: contrast recovery coefficient; SD: standard deviation; 3D: three-dimensional.

Acknowledgements

This study was supporting by Pars HMRI Hospital, India. We are also grateful for the generous help from colleagues in three hospitals who provided us with the 3 PET/CT scanners, GE scanners.

References

[1]. A NIM PET/CT Phantom For Evaluating The PET Image Quality Of Micro-Lesions And The Performance Parameters Of CT Shujie Lu†, Peng Zhang†, Chengwei Li, Jie Sun, Wenli Liu And Pu Lu Et Al. BMC Medical Imaging (2021) 21:165 Society Of Nuclear Medicine, India
[2]. Technical Publication Direction 5860378-1EN, Revision 1 EANM Physicist Guide.
[3]. Bailey DL, Townsend DW, Valk PE, Maisey MN. Positron Emission Tomogra- Phy. Berlin: Springer; 2015.
[4]. Du J, Li W, Lu K, Xiao B. An Overview Of Multi-Modal Medical Image Fusion. Neurocomputing. 2016;215:3.
[5]. Velasco C, Mota-Cobian A, Mateo J, Espana S. Explicit Measurement Of Multi-Tracer Arterial Input Function For PET Imaging Using Blood Sampling Spectroscopy. EJNMMI Phys. 2020;7(1):7.
[6]. Rahmim A, Qi J, Sossi V. Resolution Modeling In PET Imaging: Theory, Prac- Tice, Benefits, And Pitfalls. Med Phys. 2013;40:064301.
[7]. Farma JM, Santillan AA, Melis M, Walters J, Belinc D, Chen DT, Eikman EA, Malafa M. PET/CT Fusion Scan Enhances CT Staging In Patients With Pancre-Atic Neoplasms. Ann Surg Oncol. 2008;15(9):2465.
[8]. PET/CT Atlas On Quality Control And Image Artefacts. Vienna:INTERNATIONAL ATOMIC ENERGY AGENCY, 2014.
[9]. Zhang J, Maniawski P, Knopp MV. Performance Evaluation Of The Next Generation Solid-State Digital Photon Counting PET/CT System. EJNMMI Res. 2018;8(1):1–16.
[10]. Association NEM. Performance Measurements Of Positron Emission Tomo- Graphs. Published:NEMA Standards Publication NU 2-2012, 2012.
[11]. IEC. Evaluation And Routine Testing In Medical Imaging Departments—Part 3–5: Acceptance And Constancy Tests—Imaging Performance Of Computed Tomography X-Ray Equipment. Published. 2019.
[12]. Adler S, Seidel J, Choyke P, Knopp MV, Binzel K, Zhang J, Barker C, Conant S, Maass-Moreno R. Minimum Lesion Detectability As A Measure Of PET System Performance. EJNMMI Phys. 2017;4(1):13.
[13]. Bettinardi V, Presotto L, Rapisarda E, Picchio M, Gianolli L, Gilardi MC. Physical Performance Of The New Hybrid PETCT Discovery-690. Med Phys. 2011;38(10):5394.
[14]. Ziegler S, Jakoby BW, Braun H, Paulus DH, Quick HH. NEMA Image Quality Phantom Measurements And Attenuation Correction In Integrated PET/MR Hybrid Imaging. EJNMMI Phys. 2015;2(1):1–14.
[15]. Delbeke D. Oncological Applications Of FDG PET Imaging: Brain Tumors, Colorectal Cancer Lymphoma And Melanoma. J Nucl Med. 1999;40:591.
[16]. Sathiakumar C, Som S, Eberl S, Lin P. NEMA NU 2–2001 Performance Test- Ing Of A Philips Gemini GXL PET/CT Scanner. Australas Phys Eng Sci Med. 2010;33(2):199.
[17]. Gulliksrud K, Stokke C, Martinsen AC. How To Measure CT Image Quality: Variations In CT-Numbers, Uniformity And Low Contrast Resolution For A CT Quality Assurance Phantom. Phys Medica. 2014;30:521–6.
[18]. Taniguchi T, Akamatsu G, Kasahara Y, Mitsumoto K, Baba S, Tsutsui Y, Himuro K, Mikasa S, Kidera D, Sasaki M. Improvement In PET/CT Image Quality In Overweight Patients With PSF And TOF. Ann Nucl Med. 2015;29(1):71.
[19]. Armstrong IS, Kelly MD, Williams HA, Matthews JC. Impact Of Point Spread Function Modelling And Time Of Flight On FDG Uptake Measurements In Lung Lesions Using Alternative Filtering Strategies. EJNMMI Phys. 2014;1:1–18.
[20]. Ketabi A, Ghafarian P, Mosleh-Shirazi MA, Mahdavi SR, Ay MR. The Influence Of Using Different Reconstruction Algorithms On Sensitivity Of Quantitative 18F-FDG-PET Volumetric Measures To Background Activity Variation. Iran J Nucl Med. 2018;26(2):87.
[21]. Vandenberghe S, Van Elmbt L, Guerchaft M, Clementel E, Verhaeghe J, Bol A, Lemahieu I, Lonneux M. Optimization Of Time-Of-Flight Reconstruction On Philips GEMINI TF. Eur J Nucl Med Mol Imaging. 2009;36(12):1994.
[22]. Conti M, Bendriem B, Casey M, Mu C, Kehren F, Michel C, Panin V. Imple- Mentation Of Time-Of-Flight On CPS Hirez PET Scanner. In: IEEE Symposium Conference Record Nuclear Science 2004, P. 2796.
[23]. Panin VY, Kehren F, Michel C, Casey M. Fully 3-D PET Reconstruction With System Matrix Derived From Point Source Measurements. IEEE Trans Med Imaging. 2006;25(7):907.
[24]. Akamatsu G, Ishikawa K, Mitsumoto K, Taniguchi T, Ohya N, Baba S, Abe K, Sasaki M. Improvement In PET/CT Image Quality With A Combination Of Point-Spread Function And Time-Of-Flight In Relation To Reconstruction Parameters. J Nucl Med. 2020;53(11):1716.
[25]. Bao Q, Chatziioannou AF. Estimation Of The Minimum Detectable Activity Of Preclinical PET Imaging Systems With An Analytical Method. Med Phys. 2010;37(11):6070.
[26]. Schaefferkoetter J, Casey M, Townsend D, El Fakhri G. Clinical Impact Of Time-Of-Flight And Point Response Modeling In PET Reconstructions: A Lesion Detection Study. Phys Med Biol. 2013;58(5):1465.
[27]. Oen SK, Aasheim LB, Eikenes L, Karlberg AM. Image Quality And Detectability In Siemens Biograph PET/MRI And PET/CT Systems——A Phantom Study. EJNMMI Phys. 2019;6(1):16.
[28]. Raylman R, Kison P, Wahl RL. Capabilities Of Two- And Three-Dimensional FDG-PET For Detecting Small Lesions And Lymph Nodes In The Upper Torso: A Dynamic Phantom Study. Eur J Nucl Med. 1999;26:39–45.
[29]. Kadrmas DJ, Casey ME, Conti M, Jakoby BW, Lois C, Townsend DW. Impact Of Time-Of-Flight On PET Tumor Detection. J Nucl Med. 2009;50(8):1315.